International Symposium
On Turbulence and Shear Flow
Phenomena (TSFP-9)
June 30 - July 3, 2015 *Melbourne, Australia*

EXPERIMENTAL AND NUMERICAL STUDIES ON OPTIMAL SHAPE OF A SINUSOIDAL RIBLET FOR DRAG REDUCTION IN WALL TURBULENCE

Monami Sasamori[1], Oozora Iihama[1], Hiroya Mamori[1†], Kaoru Iwamoto[1*], and Akira Murata[1]

1: Department of Mechanical Systems Engineering
Tokyo University of Agriculture and Technology
2-24-16 Nakacho, Koganei, Tokyo 184-8588, Japan

† Present address: Department of Mechanical Engineering
Tokyo University of Science
6-3-1 Niijuku, Katsushika, Tokyo 125-8585, Japan

*Corresponding author: iwamotok@cc.tuat.ac.jp

BACKGROUND AND OBJECTIVES

Skin friction drag significantly increases in wall turbulence. Techniques for reducing skin friction drag are required to be developed because it is expected to decrease energy costs of transportation equipment. A well-known method for decreasing skin friction drag is installing streamwise micro grooves on wall surfaces, which are called as 'riblet surfaces'. Since riblet surfaces can be readily applied to existing equipments, so many types of 'two-dimensional riblet shapes' (refereed as 2-D riblets, hereafter) have been performed and their drag reduction effects have been confirmed, e.g., Walsh (1980); Bechert *et al.* (1997); Choi (1989). Here, the '2-D' means that the riblets are aligned in the streamwise direction. The shape of 2-D riblets has been optimized, of which drag reduction rate is approximately 10% (Bechert *et al.*, 1997). The optimized 2-D riblet is a blade-type with very thin adjacent walls, and the lateral spacing is smaller than the diameter of streamwise vortices. Choi *et al.* (1993) reported that the riblet affects ejection and sweep events and inhibits streamwise vortices approaching to near-wall regions, because the lateral spacing of the riblet is smaller than the diameter of streamwise vortices. However, riblet surfaces with higher drag reduction effect are required in order to apply riblets in practical applications, because decrease in fuel costs by the above-mentioned drag reduction effect was not sufficient to cover maintenance costs of the riblet (Viswanath, 2002).

Instead of 2-D riblets, three-dimensional riblet surfaces (3-D riblets) have also been investigated in order to obtain higher drag reduction. The '3-D' means that a riblet shape varies in the streamwise direction. One of expected riblet shapes is a wavy riblet suggested by Peet & Sagaut (2009). They aimed to obtain an effect similar to spanwise wall oscillation technique, e.g., Choi & Graham (1998). They found 7.4% drag reduction rate and concluded that decrease of crossflow turbulence contributes to drag reduction. As best of author's knowledge, obtained drag reduction rates by 3-D riblets, however, are smaller than that by the optimized 2-D riblet. It is because an optimization of the shape of 3-D riblets is difficult due to many parameters of the shape as compared with those of 2-D riblet.

In the present study, we perform a sinusoidal riblet surface which is one of 3-D riblets. The lateral spacing of adjacent walls of the sinusoidal riblet sinusoidally varies. The maximum drag reduction effects of 7.4% and 11.7% have been confirmed by a numerical (Iihama *et al.*, 2014) and an experimental (Sasamori *et al.*, 2014) investigations, respectively. Sasamori *et al.* (2014) reported that the drag-reduction mechanism is similar to those of 2-D riblets. A different point is that the sinusoidal riblet respectively induces a downward and upward flows in the expanded and contracted regions, which prevent vortices from hitting the bottom wall with wider lateral spacing of the riblet. In consequence, the wetted area of the sinusoidal riblet is smaller than those of two-dimensional riblets, resulting in the high drag-reduction effect. Yamaguchi *et al.* (2014) also reveals that the riblet deteriorates vortical structures and that advection velocity of vortices is the same as induced flow by the sinusoidal riblet in the wall-normal direction.

However, the optimal shape of the sinusoidal riblet and the effect of the shape parameters on the flow are unclear. Therefore, we set two objectives of this study: optimization of the parameters of the sinusoidal riblet shape in order to obtain a larger drag reduction effect by the sinusoidal riblet surface; investigation of the influence of the flow due to the variation of the parameter. The optimization of the shape is effectively performed by means of the combination of the numerical and experimental studies as described below.

The final goal of our study is to perform the optimized sinusoidal riblet surface. In the present study, we compare results from the parametric study by means of direct numerical simulations and an experiment. And we discuss present optimal parameter sets inducing large drag reduction effect and reveals influences of riblet parameters on the flow fields.

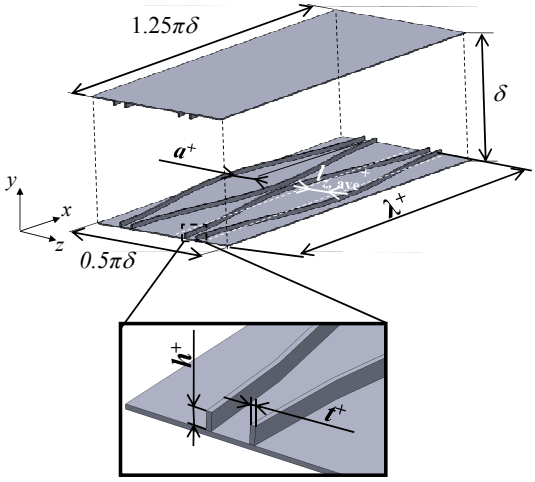

Figure 1. Computational domain of the DNS and the sinusoidal riblet surface.

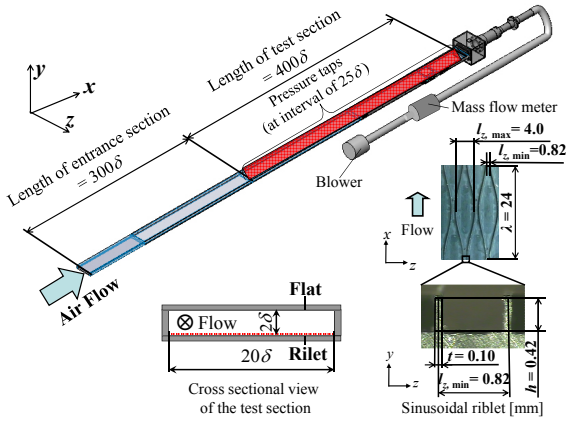

Figure 2. Schematic view of experimental apparatus.

NUMERICAL AND EXPERIMENTAL SETUPS

1 DIRECT NUMERICAL SIMULATION

Direct numerical simulations (DNSs) of a fully developed turbulent channel flow are performed. The computational domain is shown in Fig. 1. Here, the superscript of plus denotes a wall unit (i.e., nondimensionalized by the friction velocity u_τ and the kinematic viscosity ν). The governing equations are an incompressible continuity and Navier-Stokes equations. The riblet surface is installed on both the channel walls and represented by using an immersed boundary method (Kim *et al.*, 2001). The base flow is driven by a constant mean pressure gradient. A friction Reynolds number is set to be $Re_\tau = 110$, which is based on a friction velocity in the flat surface case $u_{\tau,\,\mathrm{flat}}$ and the channel half width δ. A drag reduction rate R_D is evaluated from total drag coefficients of the flat and the riblet surface cases. Periodic boundary conditions are imposed in homogeneous directions and no-slip conditions are imposed on the channel walls and the surfaces of the riblet. The number of grids is 192, 216, and 192 in the streamwise, wall-normal, and spanwise directions, respectively.

2 EXPERIMENT

Figure 2 shows an experimental setup. The wind tunnel has a rectangular cross-section of 20.0×200 mm^2 and a length of 7000 mm. The working fluid is air. To provide a fully developed turbulent flow at the inlet of a test section, the length of an entrance section is set to be 300δ in the streamwise direction and a turbulence grid is installed at the inlet of the entrance section. The length of the test section is 400δ. The channel half-width δ is 10 mm in this case. Note that the riblet plate is installed on the lower wall of the test section, in contrast to the DNSs. The total drag coefficients C_T is calculated by measuring the flow rate, the temperature and the differential pressure between two pressure taps. Drag reduction rate R_D defined as

$$R_D = \frac{C_{T,\,\mathrm{flat}} - C_{T,\,\mathrm{rib}}}{C_{T,\,\mathrm{flat}}} \times 100 \times 2, \qquad (1)$$

is evaluated from the total drag coefficient of the flat-surface case ($C_{T,\,\mathrm{flat}}$) and the riblet-surface case ($C_{T,\,\mathrm{rib}}$) with a same bulk Reynolds number Re_b.

PARAMETERS AND OPTIMIZATION

The sinusoidal riblet shape is also shown in Figs. 1 and 2. The sinusoidal riblet has five parameters: a height of the riblet wall, h^+; a thickness of the riblet wall, t^+; a wavelength of the wave, λ^+; an amplitude of the wave, a^+; an averaged lateral spacing, $l^+_{z,\,\mathrm{ave}}$.

As for DNSs, we performed a paramteric study for the height h^+, the thickness t^+, the amplitude a^+, and the wavelength λ^+. In order to avoid increasing the cost of the computation, the wavelength is up to the streamwise length of the computational domain; the averaged lateral spacing of the adjacent walls of the riblet $l^+_{z,\,\mathrm{ave}}$ is kept at constant; the friction Reynolds number is set to be constant. The parameter set of $h^+ = 7.5$, $t^+ = 1.8$, $\lambda^+ = 431.6$, $a^+ = 14.22$, and $l^+_{z,\,\mathrm{ave}} = 42.27$ is chosen as a reference case for DNSs. The parametric study is done in the ranges of $3.75 \le h^+ \le 11.25$, $1.8 \le t^+ \le 3$, $107.9 \le \lambda^+ \le 431.6$, and $4.72 \le a^+ \le 18.48$ (16 cases in a total).

In the experiment, the Reynolds number can be varied easily and it corresponds that the riblet shape varies with keeping a similarity (although it is difficult to change parameter individually). The geometry of the sinusoidal riblet is also shown in Fig. 2, of which shape parameters are determined based on the results of the present DNS The sinusoidal riblet is made from acrylonitrile butadiene styrene (ABS) resin and milled by a computer numerical control machining center. The bulk Reynolds number Re_b is varied from 2000 to 6000, which corresponds to expand the reference shape under keeping the similarity. Here, the Reynolds number Re_b is defined by a twice bulk velocity and a channel half width δ. The corresponding scaling factor is from 0.4 to 1.0.

The optimization of the parameter is done in a mutually complementary manner: the DNS clarifies optimal values of h^+, t^+, a^+ and λ^+; the riblet is manufactured based on them and we feedback the optimal parameter for the next

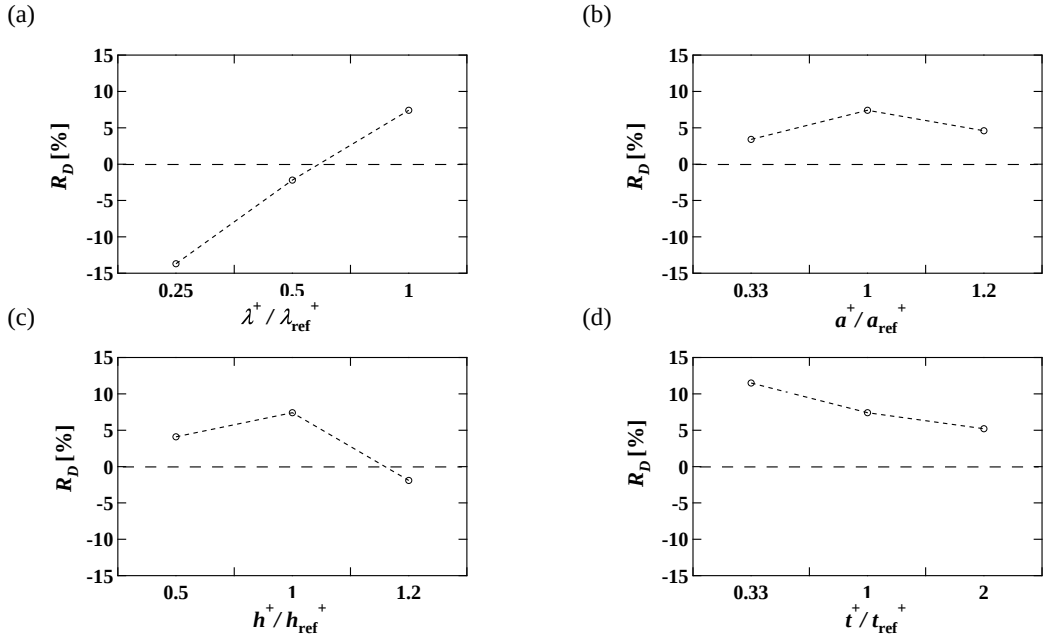

Figure 3. The total drag-reduction rate as functions of (a) wavelength, (b) amplitude, (c) height, and (d) thickness. These are obtained by the DNS.

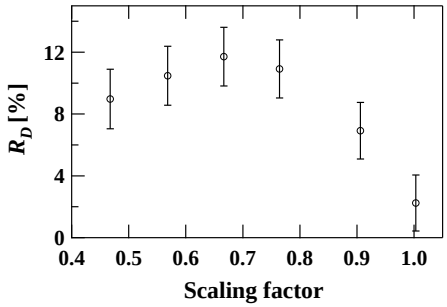

Figure 4. The total drag-reduction rate R_D as a function of the scaling factor. These are obtained by the experiment.

DNS. Repeating the DNS and the experiment, the parameters of the riblet can be approached to an optimal shape.

RESULTS

1 OPTIMAL SHAPE

Figure 3 shows the drag reduction rate as functions of parameters in the present DNSs. Parameters are scaled by those of the reference case. As increasing the wavelength shown in Fig. 3(a), the drag reduction rate increases and a maximum value is $R_D = 7.4\%$ at the reference size. The figure implies that the optimal wavelength is larger than that of the reference case, while it cannot be examined due to the limitation of the calculation domain. Figures 3(b) and (c) show the effect of the amplitude and height on R_D, respectively. The optimal amplitude and height are those of the reference case. Figure 3(d) shows the effect of the thickness. A drag reduction rate increases as decreasing the thickness, of which tendency has already been confirmed in the 2-D riblet case (Bechert *et al.*, 1997). Due to the difficulty of the manufacturing, we cannot make the riblet with the thickness of $t^+/t^+_{\rm ref} = 0.33$. Therefore, the parameter set of $h^+ = 7.5$, $t^+ = 1.8$, $\lambda^+ = 431.6$, $a^+ = 14.22$, and $l^+_{z,\,\rm ave} = 42.27$ is employed as the reference parameter set for the experiment.

Figure 4 shows the drag reduction rate as a function of the scaling factor in the experiment. If the scaling factor is doubled, all parameters are also doubled. The maximum drag reduction rate of $R_D = 11.7\%$ is confirmed at the scaling factor of 0.67. The scaling factor corresponds to the parameter set of $h^+ = 5.0$, $t^+ = 1.2$, $\lambda^+ = 285.6$, $a^+ = 9.5$, and $l^+_{z,\,\rm ave} = 28.7$. We feedback the parameter set into next DNSs as a new reference in near future.

2 FLOW FIELD

In this section, influences of the wavelength on the drag reduction rate and flow fields are discussed. The data are obtained from the present DNSs. Figure 5 shows total drag rate for different wavelength. The drag consists of contributions from the pressure drag D_p and the skin-friction drag D_f. The skin-friction drag is divided into contributions from the channel surface $D_{f,\,\rm channel\,wall}$, the riblet upper walls $D_{f,\,\rm rib\,upper}$, and the riblet side walls $D_{f,\,\rm rib\,side}$ as shown in Fig. 5(b). As decreasing the wavelength, the contribution from the pressure drag increases, while the contri-

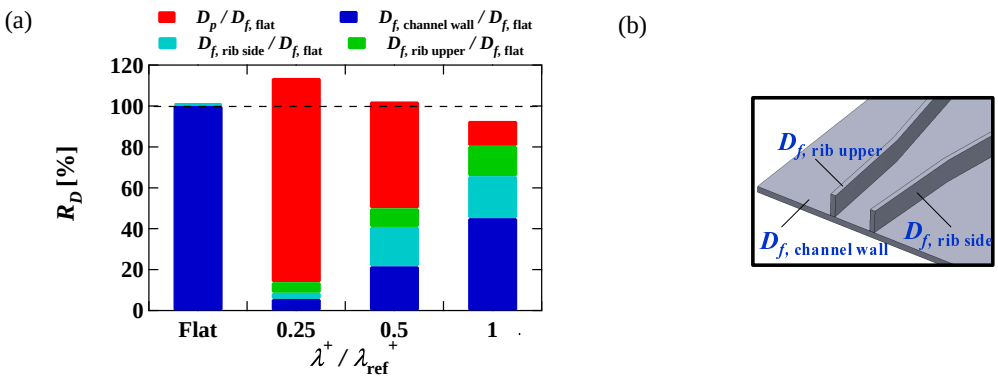

Figure 5. The drag reduction rate for different wavelength obtained by the DNSs.

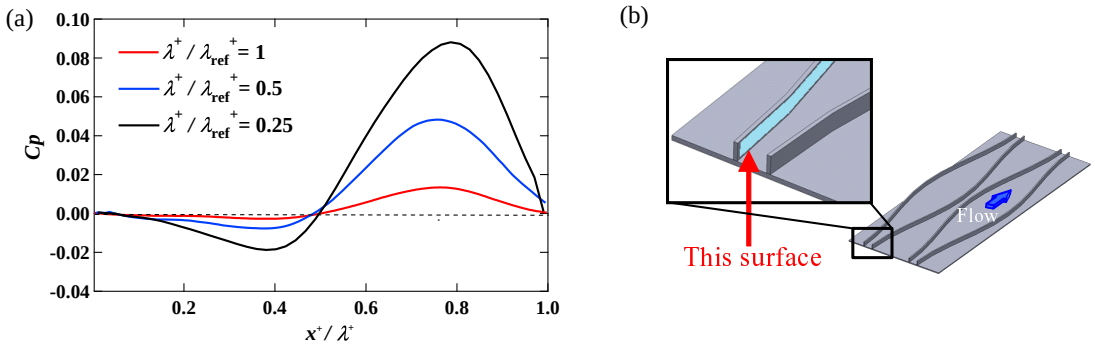

Figure 6. Profiles of the pressure drag over the riblet surface.

bution from the skin-friction drag decreases. Particularly, decreases in the contributions from the skin-friction drag on the riblet side wall and channel surface are remarkable. This is because of the flow separation and decrements of the wall shear stress and the Reynolds shear stress as described below.

Figure 6(a) shows the pressure drag profile on the riblet side wall surface (shown in Fig. 6(b)). In Fig. 6(a), the horizontal axis is the streamwise coordinate normalized by the wavelength and the vertical axis is the streamwise component of the wall pressure. The pressure drag decreases and increases where the lateral spacing of the riblet expands and contracts, respectively. As decreasing the wavelength, the increment of the pressure drag in the contracted region is larger than the decrement in the expanded region, resulting in the increment of the pressure drag in total as shown in Fig. 5(a).

Figure 7 shows profiles of the streamwise velocities averaged in the streamwise and spanwise directions, together with that of the flat case. Here, symbols of $\overline{()}$ and $\langle\rangle$ mean values averaged in time and averaged in the streamwise and spanwise directions, respectively. The streamwise velocity of the riblet case is below that of the flat case in the region near the riblet wall ($y^+ < 30$) and it decreases as decreasing the wavelength. The velocity profile indicates the decrease of the wall shear stress, which is confirmed in Fig. 8. In the case of the reference case, the high wall shear stress is observed in the center region of the riblet surface. In contrast, for the case of shorter wavelength case, the high wall shear stress area decreases and locates the lateral spacing of the riblet wall is narrow. Moreover, flow separation occurs in the case of $\lambda^+/\lambda^+_{ref}$= 0.25. These contribute to decrease the skin-friction drag on the riblet side wall and the channel surface.

According to the identity equation performed by Fukagata *et al.* (2002), the decrease in the Reynolds shear stress (refereed as the RSS, hereafter) indicates the skin-friction drag reduction. Since the present riblet varies in the streamwise direction periodically, the RSS can be decomposed into two parts:

$$-\overline{u'^+v'^+} = -\widetilde{u^+}\widetilde{v^+} - \overline{u''^+v''^+}. \qquad (2)$$

The first and second terms in the RHS are 'periodic-RSS' and 'random-RSS', respectively. Symbols of $\widetilde{()}$, $()'$, and $()''$ mean periodic fluctuation, fluctuation from the spatiotemporal average, and fluctuation from time average, respectively. Figure 9 shows the random-RSS profile averaged in the streamwise and spanwise directions. The decrease of the random-RSS is clearly observed in the case of the riblet cases. Moreover, the random-RSS in the case of $\lambda^+/\lambda^+_{ref}$= 0.25 is smaller than other profiles. Figure 10 shows the random-RSS distribution on a $y-z$ plane at the half of the wavelength. The large random-RSS is observed in the range of $20 < y^+ < 50$ and decreases as decreasing the wavelength.

In summary, the sinusoidal riblet decreases not only the wall shear stress, but also turbulence (random-RSS), resulting in the skin-friction drag reduction. In the case of the shorter wavelength, however, the increase of pressure drag exceeds the decrease of the friction drag.

CONCLUSIONS

We performed parameter optimization of a sinusoidal riblet in a fully developed turbulent channel flow by means of direct numerical simulations and experiments. We also investigated the influence of the variation of the parameter on the flow field.

1. The present optimal parameter set is the height $h^+ = 5.0$, the thickness $t^+ = 1.2$, the wavelength $\lambda^+ = 285.6$, the amplitude $a^+ = 9.5$, and the averaged lateral spacing $l^+_{z,\mathrm{ave}} = 28.7$. We feedback the parameter set into next DNSs as a new reference in order to obtain an optimal shape.

2. As decreasing the wavelength, the contribution from the pressure drag increases, while the contribution from the skin-friction drag decreases. In the case of the shorter wavelength, the increase of pressure drag exceeds the decrease of the friction drag, resulting in increase of the total drag as compared with the flat case.

3. The sinusoidal riblet decreases not only the wall shear stress, but also turbulence (random-RSS), resulting in the skin-friction drag reduction.

REFERENCES

Bechert, D. W., Bruse, M., Hage, W., Vanderhoeven, J. G. T. & Hoppe, G. 1997 Experiments on drag-reducing surfaces and their optimization with an adjustable geometry. *Journal of Fluid Mechanics* **338**, 59–87.

Choi, H., Moin, P. & Kim, J. 1993 Direct numerical simulation of turbulent flow over riblets. *Journal of Fluid Mechanics* **225**, 503–539.

Choi, K. S. 1989 Near-wall structure of a turbulent boundary layer with riblets. *Journal of Fluid Mechanics* **208**, 417–458.

Choi, K. S. & Graham, M. 1998 Drag reduction of turbulent pipe flows by circular-wall oscillation. *Physics of Fluids* **10** (1), 7–9.

Fukagata, K., Iwamoto, K. & Kasagi, N. 2002 Contribution of reynolds stress distribution to the skin friction in wall-bounded flows. *Physics of Fluids* **14** (L73), 4.

Iihama, O., Mamori, H., Iwamoto, K. & Murata, A. 2014 Drag-reduction effect of sinusoidal riblets in turbulent channel flow by direct numerical simulatio. *Proc. of 11th. World Congress on Computational Mechanics (WCCM XI)* .

Kim, J., Kim, D. & Choi, H. 2001 An immersed-boundary finite-volume method for simulations of flow in complex geometries. *Journal of Computational Physics* **171**, 132–150.

Peet, Y. & Sagaut, P. 2009 Theoretical prediction of turbulent skin friction on geometrically complex surfaces. *Physics of Fluids* **21** (105105), 19.

Sasamori, M., Mamori, H., Iwamoto, K. & Murata, A. 2014 Experimental study on drag-reduction effect due to sinusoidal riblets in turbulent channel flow. *Experiments in Fluids* **55**, 1–14.

Viswanath, P. R. 2002 Aircraft viscous drag reduction using riblets. *Progress in Aerospace Sciences* **38**, 571–600.

Walsh, M. J. 1980 Drag characteristics of v-groove and transverse curvature riblets. *Symposium on Viscous Flow Drag Reduction* **72** (207), 168–184.

Yamaguchi, K., Sasamori, M., Mamori, H., Iwamoto, K. & Murata, A. 2014 Analysis of vortical structure over a sinusoidal riblet by dual-plane stereoscopic piv. *Proc. of International Symposium on Application of Laser Techniques to Fluid Mechanics Lisbon* (119), 7.

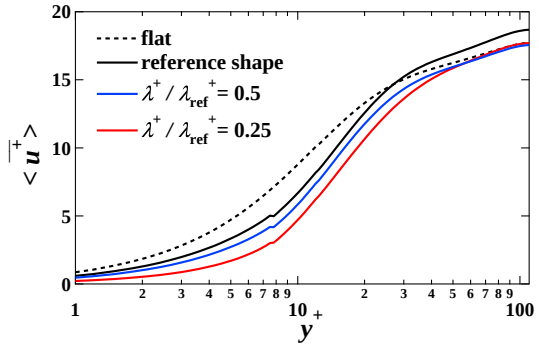

Figure 7. Profiles of the streamwise velocity averaged in time, the streamwise direction, and spanwise direction. The profiles are compared with flat case.

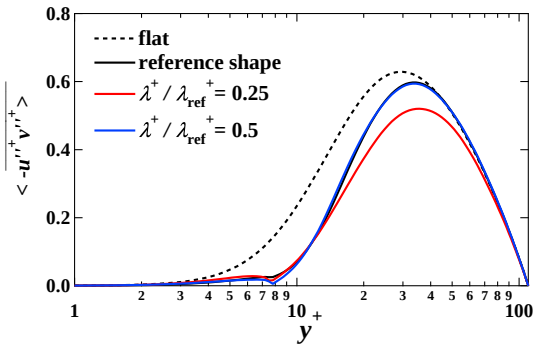

Figure 9. Profiles of the random Reynolds shear stress.

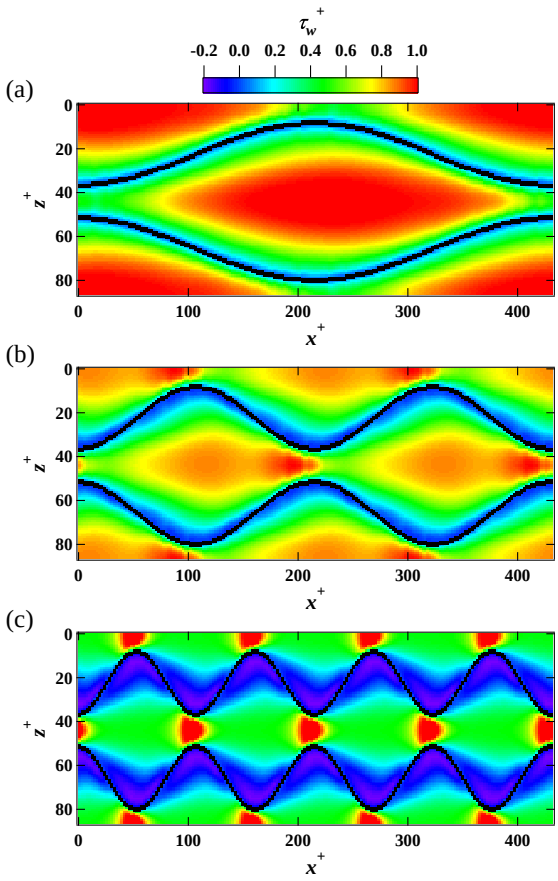

Figure 8. Distribution of the wall shear stress over the riblet surface: (a) reference case, (b) $\lambda^+/\lambda_{ref}^+ = 0.5$, (c) $\lambda^+/\lambda_{ref}^+ = 0.25$.

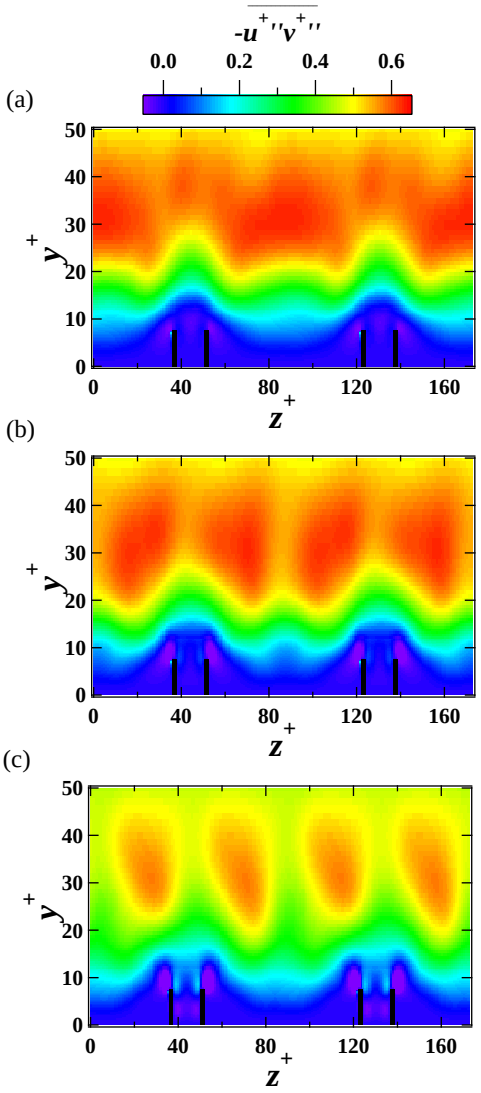

Figure 10. Distribution of the random Reynolds shear stress over the riblet surface on $y-z$ plane at $x/\lambda = 0.5$: (a) reference case, (b) $\lambda^+/\lambda_{ref}^+ = 0.5$, (c) $\lambda^+/\lambda_{ref}^+ = 0.25$.